A&A 579, A99 (2015)
DOI: 10.1051/0004-6361/201425595

Astronomy & Astrophysics

A radio map of the colliding winds in the very massive binary system HD 93129A

P. Benaglia[1,⋆], B. Marcote[2], J. Moldón[3], E. Nelan[4], M. De Becker[5], S. M. Dougherty[6], and B. S. Koribalski[7]

[1] Instituto Argentino de Radioastronomía, CCT-La Plata, CONICET, Argentina
e-mail: paula@iar-conicet.gov.ar
[2] Departament d'Astronomia i Meteorologia, Institut de Ciències del Cosmos, Universitat de Barcelona, IEEC-UB, Martí i Franquès 1, 08028 Barcelona, Spain
[3] ASTRON Netherlands Institute for Radio Astronomy, Postbus 2, 7990 AA Dwingeloo, The Netherlands
[4] Space Telescope Science Institute, 3700 San Martin Dr., Baltimore, MD 21218, USA
[5] Department of Astrophysics, Geophysics and Oceanography, University of Liège, 17 Allée du 6 Août B5c, 4000 Sart Tilman, Belgium
[6] NRC Herzberg Astronomy and Astrophysics, DRAO, PO Box 248, Penticton B.C., V0H 1K0, Canada
[7] Australia Telescope National Facility, CSIRO Astronomy & Space Science PO Box 76, Epping, NSW 1710, Australia

Received 29 December 2014 / Accepted 25 March 2015

ABSTRACT

Context. Radio observations are an effective tool for discovering particle acceleration regions in colliding-wind binaries through detection of synchrotron radiation. Wind-collision region (WCR) models can reproduce the radio continuum spectra of massive binaries. However, key constraints for models come from high-resolution imaging. Only five WCRs have been resolved to date at radio frequencies on milliarcsec (mas) angular scales. The source HD 93129A, a prototype of the very few known O2 I stars, is a promising target for study. Recently, a second massive, early-type star about 50 mas away was discovered, and a non-thermal radio source was detected in the region. Preliminary long-baseline array data suggest that a significant fraction of the radio emission from the system comes from a putative WCR.
Aims. We seek evidence that HD 93129A is a massive binary system with colliding stellar winds that produce non-thermal radiation through spatially resolved images of the radio emitting regions.
Methods. We completed observations with the Australian Long Baseline Array (LBA) to resolve the system at mas angular resolutions and reduced archival Australia Telescope Compact Array (ATCA) data to derive the total radio emission. We also compiled optical astrometric data of the system in a homogeneous way. We reduced historical *Hubble* Space Telescope data and obtained absolute and relative astrometry with milliarcsec accuracy.
Results. The astrometric analysis leads us to conclude that the two stars in HD 93129A form a gravitationally bound system. The LBA data reveal an extended arc-shaped non-thermal source between the two stars, which is indicative of a WCR. The wind momentum-rate ratio of the two stellar winds is estimated. The ATCA data show a point source with a change in flux level between 2003-4 and 2008-9, which is modeled with a non-thermal power-law spectrum with spectral indices of -1.03 ± 0.09 and -1.21 ± 0.03, respectively. The mass-loss rates derived from the deduced thermal radio emission and from the characteristics of the WCR are consistent with estimates derived by other authors.

Key words. binaries: general – stars: massive – stars: mass-loss – stars: winds, outflows – radiation mechanisms: non-thermal – radio continuum: stars

1. Introduction

Wind-collision regions (WCR) in binary systems with two hot massive stars constitute natural laboratories for studying relativistic particles (Eichler & Usov 1993; Benaglia & Romero 2003; Pittard & Dougherty 2006; De Becker 2007), as do supernova remnants but with somewhat different physical and geometrical parameters. A WCR is the site of particle acceleration that generates a population of relativistic electrons, as has now been demonstrated in more than 40 massive binary systems. The particle-accelerating colliding-wind binary (PACWB) status of these objects is, in most cases, revealed by radio observations through the detection of synchrotron emission (De Becker & Raucq 2013).

WCR models are able to reproduce the radio continuum spectra of these massive binaries (Pittard & Dougherty 2006). The radiation from these systems is the superposition of thermal emission from the stellar winds of each binary component and the non-thermal emission from the WCR. A key ingredient for constraining models of the non-thermal component is expected to come from high-resolution radio imaging. The non-thermal emission region associated with colliding winds has been mapped at radio frequencies for WR 140 (Dougherty et al. 2005), WR 146 (O'Connor et al. 2005), WR 147 (Williams et al. 1997), Cyg OB2 #5 (Contreras et al. 1997; Ortiz-León et al. 2011), and Cyg OB2 #9 (Dougherty & Pittard 2006). In each case, the WCR is resolved by observations with angular resolutions of a few milliarcseconds (mas).

HD 93129A is the brightest source in the most crowded part of Tr 14 in the Carina nebula, and it has been studied for several

⋆ Fellow of CONICET.

decades. The record of its special spectral characteristics can be traced back to Payne (1927) (see also Table 1 for information on other studies). It now is recognized as hosting the prototype O2 If* (Walborn et al. 2002). Radio emission from HD 93129A has been detected between 1.4 and 24.5 GHz (e.g., Benaglia et al. 2006), showing a flux that decreases with a frequency indicative of synchrotron radiation, most probably produced in a WCR between stars in a colliding-wind binary system. The Australian Long Baseline Array (LBA)[1] observation presented by Benaglia et al. (2010) suggests that a significant fraction of the radio emission comes from a region compatible with a WCR.

In this paper, we offer an in-depth discussion of a more recent LBA observation of HD 93129A, aiming to provide compelling evidence of the WCR origin for the bulk of the radio emission, in agreement with the so-called standard scenario for PACWBs. These results allow us to spatially resolve the synchrotron emission region for the first time and to derive specific information about the non-thermal radio contribution. The two-component nature of HD 93129A is presented, including the most recent astrometric measurements that show the relative position of the components over time (Sect. 2) and a new analysis of *Hubble* Space Telescope/Fine Guidance Sensor (HST/FGS) data that allows us to correlate the optical positions of the two components with the position of the radio emission (Sect. 3). The LBA observations are presented in Sect. 4. The main results and general discussion are in Sects. 5 and 6, with a final statement of our conclusions in Sect. 7.

2. The HD 93129A stellar system

The object HD 93129A was first classified as an O3 star (Walborn 1982), though was later reclassified as the prototype O2 I star (Walborn et al. 2002). Mason et al. (1998) suggested it was a speckle binary, and this was confirmed as having two components, Aa and Ab, from HST/FGS observations (Nelan et al. 2004). These authors provide the separation at the epoch of the observations, the difference in apparent visual magnitude between the primary and the secondary, and the position angle (PA; see also Nelan et al. 2010). Maíz Apellániz et al. (2008) detected proper motion along the radius vector between the components after analysis of data from 1996, 2002, and 2004: the binary nature is supported by the relative velocity of about 2 mas yr^{-1}, higher than the expected relative velocities in the field. The authors suggest a highly elliptical or inclined orbit, or both, although they did not determine the orbital parameters. The companion is assumed to be coeval with the primary and to have the same spectral type as various other OB stars nearby (O3.5 V) (see Table 1). Through detailed ultraviolet and Hα line modeling, Taresch et al. (1997) and Repolust et al. (2004) derived the main parameters of HD 93129A (see Table 1).

The relative motion of the two stars can be traced by archived HST/FGS and HST/ACS[2] observations from 1996 to 2009, along with the recent VLT/NACO and VLTI/PIONIER[3] observations of Sana et al. (2014). Figure 1 shows the relative astrometry from these measurements over time. The position angles for 1996 and 2002 have large uncertainties because the binary components were resolved along only one FGS axis, owing to the HST roll angle resulting in a small projected separation along the unresolved axis. For later epochs, the approximate position angle was known, so the observations were planned to avoid this problem.

HD 93129A was included in the recent Galactic O star Spectroscopic Survey of Sota et al. (2014). The coordinates from the Tycho catalog (Høg et al. 2000) assume a single star, since the presence of a companion star was unknown at the time. HIPPARCOS did not resolve the system. These coordinates have errors of about 0.1", which is an order of magnitude larger than the expected angular resolution of the LBA data of ~10 mas.

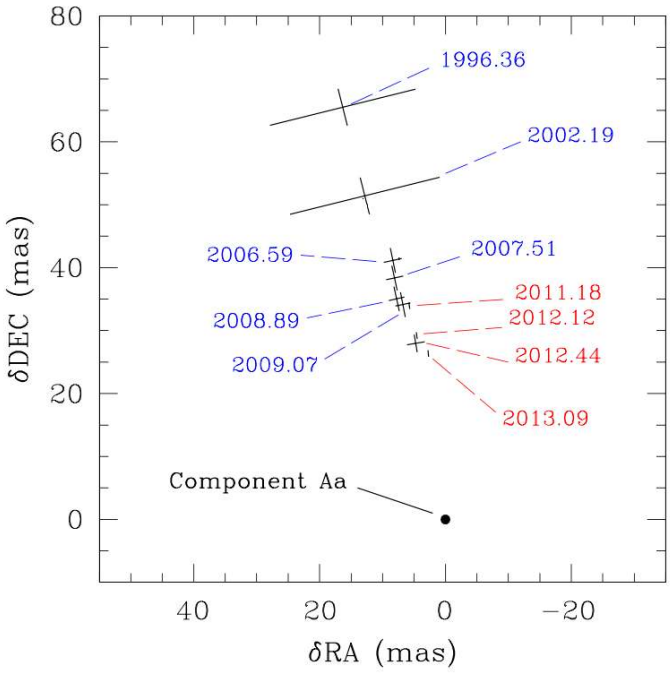

Fig. 1. Relative positions, including error bars, of the two components of HD 93129A, rederived from archive HST/FGS (blue labels) along with VLT/NACO and VLTI/PIONIER (red labels: taken from 2011.18 to 2013.09) data (Sana et al. 2014). The epoch of the measurement is given for each point.

Table 1. Adopted parameters of HD 93129A that are relevant here.

Parameter	Value	Unit	Ref.
Aa spectral type	O2 If*		Wal02
Ab spectral type	O3.5 V		Ben06
Δm	0.9 ± 0.05	mag	Nel10
Wind terminal velocity†	3200 ± 200	km s^{-1}	Tar97
System mass	200 ± 45	$M_{\odot}$	Mai08
Effective temperature†	42500	K	Rep04
System luminosity (log)	6.2	$L/L_{\odot}$	Rep04
X-ray luminosity††	1.3×10^{-7}	$L_{\rm bol}$	Coh11
Distance	2.5	kpc	Wal95

Notes. $^{(\dagger)}$ Derived if a single star. $^{(\dagger\dagger)}$ Derived from the energy band (0.5–8) keV.

References. Wal02: Walborn et al. (2002); Ben06: Benaglia et al. (2006); Nel10: Nelan et al. (2010); Tar97: Taresch et al. (1997); Mai08: Maíz Apellániz et al. (2008); Rep04: Repolust et al. (2004); Coh11: Cohen et al. (2011); Wal95: Walborn (1995).

[1] The Australian Long Baseline Array is part of the Australia Telescope, which is funded by the Commonwealth of Australia for operation as a National Facility managed by CSIRO.

[2] *Hubble* Space Telescope/Advanced Camera for Surveys.

[3] Very Large Telescope NAos-COnica and Precision Integrated-Optics Near-infrared Imaging ExpeRiment.

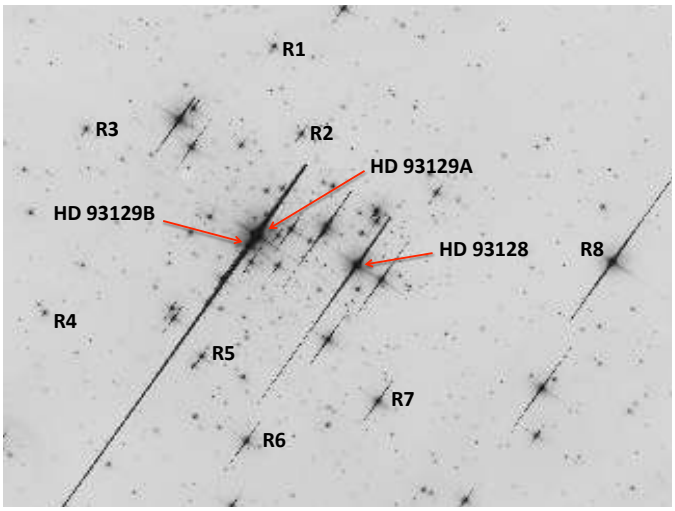

Fig. 2. Core of Tr 14 and the selected FGS reference stars used in the astrometric measurements. The image (in log stretch) is from HST proposal 10 602 using ACS/WFC with F550M, which is similar to the central pass band of the FGS measurements. The two stars HD 93129A and HD 93129B, separated by 2.7", are not clearly resolved in this image since the roll angle of HST at the time caused their position angle to be aligned with the diffraction spike. In this image the components of HD 93129A are not resolved. The separation between HD 93129A and HD 93128 is about 24". North is up and east to the left.

3. *Hubble* Space Telescope/FGS data analysis

3.1. Astrometry

To improve upon the coordinates of HD 93129A from the Tycho catalog, we analyzed HST/FGS measurements again. The three Fine Guidance Sensors on the HST are two-channel (x,y) white-light shearing interferometers that provide line-of-sight positional measurements of guide stars to enable accurate pointing and stabilization of the HST. The FGS is capable of resolving sources down to ~15 mas when operated in its high angular TRANS (or transfer) mode and submillarcsecond astrometry when operated in POS (or position) mode. A description of the FGS and its operation can be found in Nelan (2014).

In eight epochs between 2006 and 2009, FGS observed HD 93129A in TRANS mode, along with "wide angle" POS-mode observations of the binary itself and seven reference field stars within one arcminute (see Fig. 2). The TRANS mode observations resolve HD 93129Aab, providing the component separation, position angle, and magnitude difference at each epoch. The POS-mode observations supply the relative positions of the field stars and composite HD 93129A system. Combining data from these two observing modes gives the position of Aa and Ab relative to these field stars at each epoch. Combining all epochs yields a local FGS catalog of the relative positions and proper motions of reference stars and binary components.

Figure 3 shows the interference fringes of HD 93129A for the Jan 27, 2009 observations, the best fitting binary star model, and the fringes of an unresolved point source for comparison. The binary model considers the light contributed by HD 93129B, which 2.73" away, accounts for about five percent of the light of HD 93129A. (FGS optics collimates a source onto a circular beam with a full width-half maximum intensity diameter of about 3".) Figure 3 also shows the location on the fringes that the POS mode observations of HD 93129A "lock" on to. The model fit to the TRANS mode observations provides the offset

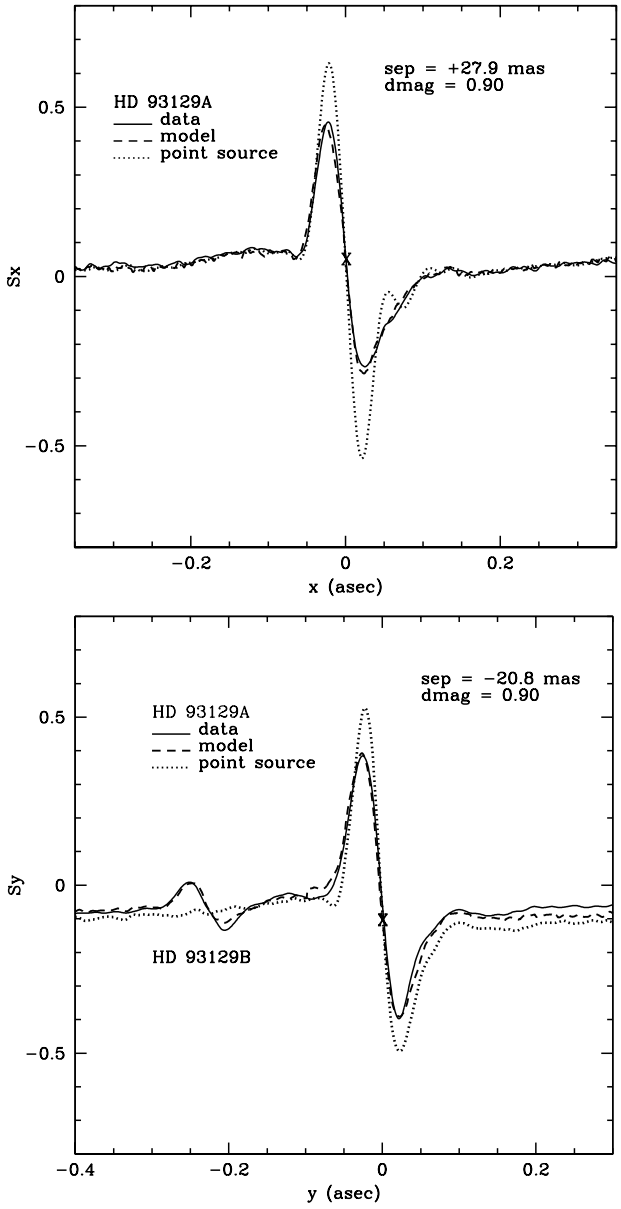

Fig. 3. Interference fringes of HD 93129A for Jan. 27, 2009 FGS observations (solid line), the best fitting binary star model (dashed line), and for comparison, the fringes of an unresolved point source (dotted line). The "X" shows the location of the composite fringe that POS mode observations tracked. Owing to the roll of HST at the time of the observations, HD 93129B has a projected separation from A along the y-axis of only 0.233″, although its true distance is 2.73″.

of each component from this point, which thereby allows us to create pseudo POS-mode exposures for both HD 93129Aa and HD 93129Ab, hence accurate positions for each star relative to the reference stars. The bright O star HD 202124 was used as the point-source calibrator since it is nearly the same $B - V$ color as HD 93129A, and it was observed by FGS only eight days after HD 93129A. The orientation of HST at the time of the observation caused the projected separation of HD 93129A and B along the FGS y-axis to be only 0.233″, as is evident in the figure.

To compare the FGS coordinates of HD 93129Aab to the radio source, it is necessary to convert the relative FGS positions to absolute International Celestial Reference System (ICRS) coordinates. The FGS coordinate frame lies in a tangential plane, with the zero point arbitrarily set to the point mid way between

Table 2. PPMXL and FGS astrometry of the HD 93129A field.

	PPMXL				FGS			
Star	RA (h)	Dec (deg)	μ_α	μ_δ	ξ	η	μ_α	μ_δ
R1	10.7325347 (13)	−59.535576 (19)	−6.6 (2.5)	−0.6 (2.5)	−2.6531 (0.9)	43.2955 (0.5)	−5.78 (0.29)	1.54 (0.31)
R2*	10.7322835 (14)	−59.541006 (16)	–	–	−9.5351 (1.0)	23.4780 (0.5)	−5.78 (0.53)	1.71 (0.50)
R3	10.7340882 (13)	−59.541208 (19)	−4.8 (3.2)	0.6 (3.2)	39.9186 (1.2)	23.1199 (0.5)	−6.73 (0.32)	1.38 (0.36)
R4	10.7344007 (49)	−59.552781 (74)	24.6 (17)	60.5 (17)	48.0711 (1.1)	−19.2493 (0.5)	−5.34 (0.44)	2.22 (0.45)
R6	10.7326563 (13)	−59.560735 (19)	−4.8 (2.1)	3.0 (2.1)	0.8902 (1.2)	−47.2647 (0.4)	−6.29 (0.32)	1.64 (0.34)
R7	10.7315615 (13)	−59.557925 (19)	−6.6 (2.5)	1.6 (2.5)	−29.0924 (1.1)	−37.1969 (0.2)	−5.46 (0.29)	1.60 (0.30)
R8	10.7296359 (15)	−59.548569 (15)	−6.4 (2.0)	2.5 (2.0)	−81.8936 (1.6)	-3.6759 (0.3)	−5.53 (0.32)	2.12 (0.30)

Notes. "Star": Reference star identification, same as in Fig. 2. All errors are shown within parenthesis. PPMXL coordinates (J2000): RA in hours, Dec in degrees, with errors in mas. The J2000 FGS tangential plane coordinates, ξ, η, are given in arcsec, relative to the point midway between the binary components; errors are in mas. Proper motions (μ) in mas yr^{-1}, with errors in the same unit. (*) Reference star 2 is not in the PPMXL catalog, so coordinates from UCAC4 are quoted. The FGS proper motions are based upon FGS data but are constrained by the PPMXL values. The entries in this table serve as the input values for the tangent plane analysis outlined in Sect. 3.

the binary components (at the zero point the FGS Cartesian plane is tangential to the celestial sphere). We used the PPMXL catalog[4] (Roeser et al. 2010) for the coordinates and proper motions of the reference stars as input to a model that finds the RA, Dec of this tangent point. This is a two-step process. The FGS observations were obtained between 2006 and 2009, while the PPXML coordinates are epoch J2000. The proper motions of the reference stars must be taken into account for the most accurate correlation of the FGS data with the radio observations. However, the proper motions provided by PPMXL have large errors. As is standard in FGS astrometry (e.g., Nelan & Bond 2013; Benedict et al. 2007), the PPMXL proper motions are input as "observations with errors" into the model that combines the FGS astrometry from the eight epochs onto the master plate. The model, which applies a four-parameter plate solution, outputs the best fitting proper motion for each reference star, based upon the FGS measurements but constrained by the PPMXL input values. The proper motions for HD 93129Aa and HD 93129Ab were solved directly without any external constraints. Table 2 lists the reference star identifier, PPMXL coordinates, and proper motions with the catalog errors, along with the resulting FGS tangent plane coordinates and proper motions and errors. The positional errors for RA, Dec are in mas, while the proper motion errors are in mas yr^{-1}. The FGS ξ, η coordinates are in arcsecs, and their errors are in mas. The FGS proper motions are now absolute rather than relative. We note that PPMXL does not contain reference star R2. For this star we used the UCAC4 (Fourth US Naval Observatory CCD Astrograph Catalog) coordinates but solved for the proper motion using only FGS data.

The next step is to find the RA,Dec of the zero point of the FGS tangential plane. The accurate FGS proper motions are used to update the PPMXL coordinates to epoch 2009, which is the epoch of the FGS master plate. Using the algorithms outlined in Smart (1960), (1) initial values for the RA, Dec of the FGS tangent point are given, for which the Guide Star Catalog v2.3 coordinates of HD 93129A are used; (2) the PPXML (RA, Dec) of each reference star are converted to Cartesian coordinates in this tangential plane, which are treated as "observations with errors"; (3) the PPXML Cartesian coordinates are used to set the scale and orientation of the FGS frame to (east, north); (4) an iterative process is applied to find a global solution that provides the best fit of the observed FGS and PPMXL coordinates in the tangential plane. The solution creates a hybrid FGS-PPMXL catalog and computes the RA, Dec of the tangent point. Once convergence is achieved, it is a straightforward process to compute the (RA, Dec) of any point in the FGS frame. We used the GAUSSFIT (Jefferys et al. 1987) least-squares program to build the models to carry out these calculations.

We compute the RA, Dec of the HD 93129Aa and Ab components, adjusted for proper motion to the Aug 6, 2008 epoch of the radio observations, equinox J2000:

$$\alpha, \delta(\mathrm{Aa}) = 10^{\mathrm{h}}43^{\mathrm{m}}57.455^{\mathrm{s}}, -59^\circ32'51.36'',$$
$$\alpha, \delta(\mathrm{Ab}) = 10^{\mathrm{h}}43^{\mathrm{m}}57.456^{\mathrm{s}}, -59^\circ32'51.33''.$$

The uncertainty in each coordinate is ±27 mas, dominated by the PPMXL catalog errors in the position and proper motion of the seven FGS reference stars surrounding HD 93129A. However, the position of Aa relative to Ab is accurate to about 1 mas. From these positions, the separation and position angle of Aab in Aug 2008 was 36 ± 1 mas and PA = 12 ± 1°.

The proper motions derived from the FGS data are μ_α, μ_δ(Aa) = −8.4, 2.6 mas yr^{-1} and μ_α, μ_δ(Ab) = −9.0, 0.0 mas yr^{-1}. The proper motion of the binary's components include any putative orbital motion along with the system motion. The difference from the reference star proper motions (Table 2), particularly in RA, could reflect internal motion within the core of Tr 14, while the reference stars lie outside the core.

3.2. Orbit estimation

The relative motion of the components Aa and Ab hints at HD 93129A being a gravitationally bound system. However, the relative positions shown in Fig. 1 cover a rather small part of the orbit and thus are inadequate for performing a standard determination of orbital elements. No definitive radial velocity variation has been reported, which is not surprising given the wide separation and apparent near linear trajectory of the stars. Nevertheless, a first approximation of an orbital fit was attempted (Fig. 4). An algorithm that minimizes the weighted square distance between the measured data points and the fitted orbit (Casco & Vila, priv. comm.) was used to determine a preliminary set of orbital parameters. Our results suggest an orbital period on the order of 200 years, an eccentricity greater than 0.9, and semi-major axes of about 93 and 37 mas, respectively, for components a and b. Our best-fit solution also points to a periapsis argument of about 220 degrees and an inclination of about 103 degrees. An attempt to fix the inclination value close to zero yielded a much poorer fit

[4] PPMXL is a catalog of positions, proper motions, 2MASS, and optical photometry of 900 million stars and galaxies.

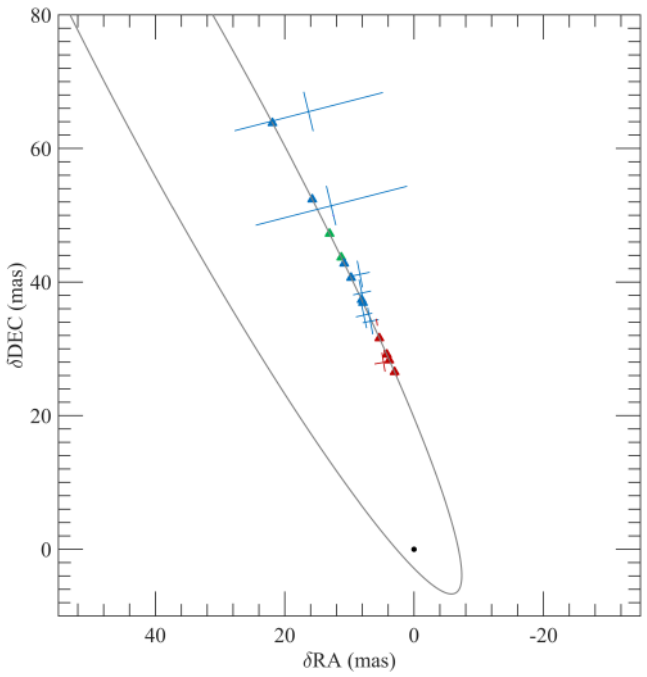

Fig. 4. Preliminary fit for the orbit (triangles: same dates as in Fig. 1 in blue and red plus 2004.6 and 2006.2 in green). The primary Aa is at the origin, The different positions of the secondary Ab between 1996 and 2013 are represented with crosses, and are the same as in Fig. 1. The figure shows the projection of the preliminary orbit in the plane of the sky.

(larger weighted root mean square rms). According to this preliminary solution, the next periastron passage is expected to take place in 2024. It should be emphasized that such a preliminary solution was calculated to give a rough idea of the orbit, even though the present astrometry does not allow for a convincing characterization of the orbit accompanied by relevant error bars on the estimated parameters. This calculation has, however, the merit of providing a preliminary basis to organize future observation campaigns dedicated to HD 93129A.

4. Radio observations

4.1. Observations of June 22, 2007

We observed HD 93129A on June 22, 2007 (MJD 54 273) between 03:00 and 13:00 UTC at 2.3 GHz as part of the eVLBI experiment vt11D3 that used Parkes, Mopra, and Australia Telescope Compact Array (ATCA) to search for suitable phase calibrators near the target (Benaglia et al. 2010). The sources PKS 0637−752 (J0635−7516) and J1047−6217 were used as flux and phase calibrators, respectively. The total time observing HD 93129A was three hours.

Standard VLBI calibration procedures were used (see also Sect. 4.2), and the source imaged with a synthesized beam of 0.2″ × 0.05″, PA = 30.9°. The source has a measured flux density of ∼3 mJy. See more details in Benaglia et al. (2010) and Fig. 5.

4.2. Observations of August 6, 2008

Further observations were conducted on Aug. 6, 2008 (MJD 54 684) from 01:00 to 12:00 UTC with the LBA at an observing frequency of 2.3 GHz, and using five antennas: ATCA (in tied-array mode, i.e., working as a single station), Parkes, Mopra, Ceduna, and Hobart (experiment V191B). The baseline lengths range from 100 to 1700 km, providing an angular resolution of ∼15 mas at that frequency. The data were recorded at 256 Mbps provided by four sub-bands of 16-MHz bandwidth at each of the two circular polarizations. The data were correlated with the Distributed FX (DiFX) software correlator located at Curtin University of Technology (WA, Australia), using 128 channels per sub-band, each band 125 kHz wide, and using two-second integrations. The data from the ATCA antennas were also correlated as an independent interferometer to obtain the total flux density from a low-resolution observation. The time on HD 93129A amounted to 3.2 h. The *uv* coverage is shown in Fig. 6.

The data reduction was performed using the Astronomical Image Processing System (AIPS)[5] software package. Bad data were flagged using telescope a priori flag files and information

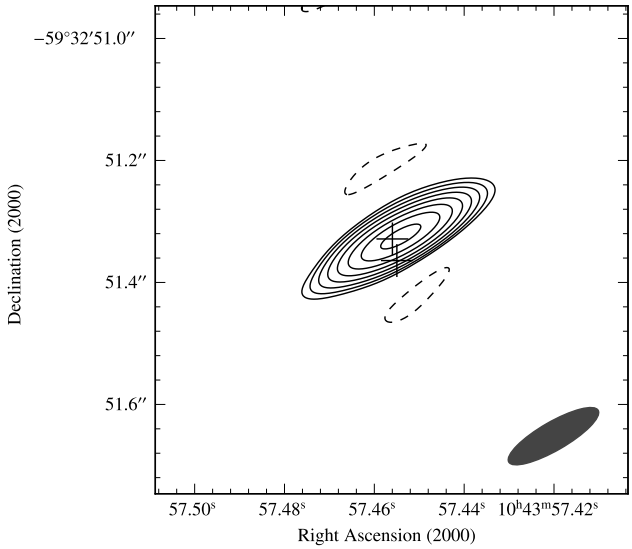

Fig. 5. HD 93129Aab system from 2007 LBA data (in contours) and location of stars Aa (southern) and Ab (northern) marked with crosses. The contours start at 0.3 mJy beam^{-1} (3σ) and increase by factors of $2^{1/2}$. The synthesized beam (0.2″ × 0.05″, PA = 31°) is shown in the bottom right corner. North is up and east to the left.

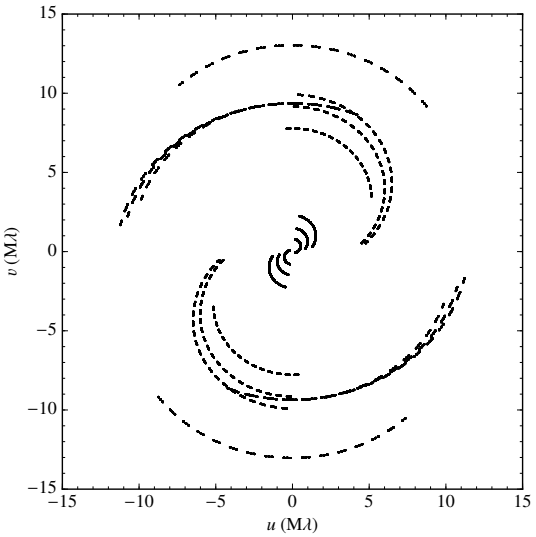

Fig. 6. *uv* coverage of project V191B in Aug. 2008.

[5] http://www.aips.nrao.edu

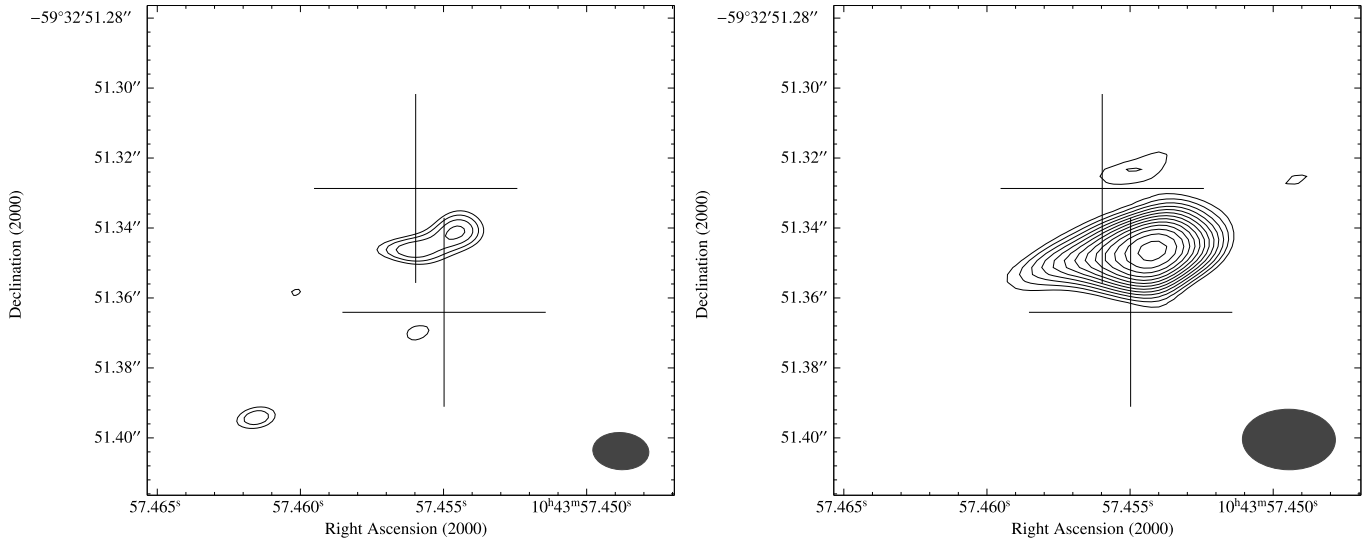

Fig. 7. LBA observations of HD 93129A at 2.3 GHz. **a)** *Left*: at highest angular resolution with an image rms of 0.21 mJy beam^{-1} and contour levels shown for −0.6, 0.6 (3σ), 0.7, 0.8, and 0.9 mJy beam^{-1}. **b)** *Right*: a tapered image that increases the weight of the shorter baselines and increases sensitivity to larger scale emission; the image rms is 0.13 mJy beam^{-1} and the contour levels are −0.4, 0.4 (3σ), 0.6, 1, 1.4, and 1.8 mJy beam^{-1}. The synthesized beams are 15 mas × 11 mas and 31 mas × 23 mas, respectively, shown in the bottom righthand corner of the images. The crosses mark the positions of the system components Aa (south) and Ab (north), at the epoch of the radio observations based on the position derived in Sect. 2. North is up and east is to the left.

provided in the observing logs. The amplitude calibration was performed using the antenna system temperatures, and phase solutions on the calibrators were obtained using the AIPS task FRING. The compact source J1047−6217 was used as the phase calibrator. The fringe finders 0637−752 (J0635−7516), 1549−790, J1051−6518, J1023−6646, and the phase calibrator J1047−6217 were used for the bandpass calibration. First, an accurate model of the calibrator was obtained after several self-calibration and imaging cycles. The calibrator, slightly resolved on the longest baselines, had a flux density of 0.99 ± 0.02 Jy. Finally, the phase solutions and the amplitude scale were transferred to the target source and images produced by deconvolving the visibility data.

The data from ATCA were correlated in standard interferometer mode. The resulting fluxes for the phase calibrator J1047-6217 and HD 93129A were 1.300 ± 0.002 Jy and 7.5 ± 0.1 mJy, respectively. The flux and uncertainty for the phase calibrator were derived by fitting a point source to the image, using all baselines.

4.3. ATCA observations

The Australia Telescope Online Archive (ATOA) was searched for observations of HD 93129A. In addition to project C678 (Benaglia et al. 2006) and the observations associated with the LBA projects described in the previous section, project C1726 targeted HD 93129A for 3.3 h at 4.8 and 8.6 GHz. Table 3 summarizes the dates and observing frequencies for these observations. In all observations with the ATCA, HD 93129A is not resolved by ATCA and appears as a point source.

5. Results

5.1. Radio flux density

In Fig. 7 we show the radio image from LBA 2008 observations of HD 93129A at 2.3 GHz. Two final images are presented: one at maximum angular resolution (Fig. 7-left: high-resolution image), and a second one using tapering that increases the sensitivity to larger scale emission (Fig. 7-right: low-resolution image). The high-resolution image has a root mean square (rms) of 0.21 mJy beam^{-1} and shows a "comma-shaped" extended emission with a flux density of 1.5 ± 0.5 mJy. The value quoted for the error is the difference in the integrated fluxes above 2 and 3σ, where σ is the measured rms of the image. In the low-resolution image, the rms noise is lower, and more flux is recovered from the source, as expected. The rms of the image is 0.13 mJy beam^{-1}, and a Gaussian fit to the source gives an integrated flux density detected by the LBA of 2.9 ± 0.5 mJy with a peak intensity of 1.8 ± 0.2 mJy beam^{-1}.

We note that the amplitude calibration of the data, which is based on the system temperature of the antennas, is limited by

Table 3. Radio flux density of HD 93129A at different frequencies obtained with ATCA and LBA data.

Array/project and date	ν [GHz]	S_ν [mJy]	Flux cal name	$S_{\nu,\mathrm{cal}}$ [Jy]
ATCA/C678				
2003-01-28	4.8	4.1 ± 0.4[a]	1934−638	2.84
2003-01-28	8.6	2.0 ± 0.2[a]	1934−638	5.83
2003-12-20	1.4	9.4 ± 0.9[a]	1934−638	14.98
2003-12-20	2.4	7.8 ± 0.4[a]	1934−638	11.59
2004-05-05	17.8	1.8 ± 0.15[a]	Mars	
2004-05-05	24.5	1.5 ± 0.35[a]	Mars	
ATCA/V191B				
2008-08-06	2.3	7.5 ± 0.11	0637−752	5.32
ATCA/C1726				
2009-01-18	4.8	5.6 ± 0.3	1934−638	5.83
2009-01-18	8.6	2.9 ± 0.3	1934−638	2.86
LBA/V191B				
2008-08-06	2.3	2.9 ± 0.51[b]	0637−752	

Notes. We include the project code and the flux density calibrator name with its flux value. [(a)] Benaglia et al. (2006); [(b)] Derived from image portrayed in Fig. 7-right.

the uncertainty on the antennas' response and gain curves. The flux density measured for the phase calibrator is ∼30% lower than its unresolved flux density measured with ATCA between Feb. 2007 and Nov. 2008: 1.46 ± 0.01 Jy to 1.42 ± 0.02. This indicates that this calibrator is partially resolved by the LBA or is variable, or both. We also note that the LBA-measured flux of HD 93129A is ∼35% of the total flux measured in simultaneous Aug 2008 ATCA data at 2.3 GHz. We conclude that the rest of the flux from HD 93129A is resolved out by the LBA.

5.2. Radio morphology and astrometry

From the 2008 LBA image, the angle subtended by the emitting source as seen from the secondary star (so-called opening angle $2\theta_w$) can be estimated, leading to half-opening angle $\theta_w \sim 65°$. This is related to the wind-momentum rate ratio η by $\theta_w = 180° \times \eta/(1+\eta)$, thus implying $\eta \sim 0.6$.

The radio emission at maximum angular resolution presents two maxima. The position of the centroid of the two fitted Gaussians is α_C = 10:43:57.456, δ_C = −59:32:51.34, J2000.

A systematic uncertainty of 1.1 mas in right ascension and 2.8 mas in declination comes from the position error of the phase reference calibrator in the ICRF2 (International Celestial Reference Frame, second realization). Therefore, the absolute uncertainty of the position of the radio emission is about 3 mas in the ICRF. Figure 7 shows the positions of HD 93129 Aa and Ab, with the size of the crosses indicating the absolute uncertainty, although the relative separation of the components has an uncertainty of ∼ 1 mas (see Sect. 3).

6. Discussion

6.1. Wind-momentum rates

The radio source appears in the LBA observations as a bow-shaped region, slightly curved around component Ab and reminiscent of the WCRs resolved in WR 140 (Dougherty et al. 2005), WR 146 (O'Connor et al. 2005), Cyg OB2 #5 (Ortiz-León et al. 2011), as examples. If we assume that the radio source is centered on the stagnation point of the WCR, the wind momentum rates ratio η can be expressed as

$$\eta = \left(\frac{R_b}{R_a}\right)^2 = \frac{\dot{M}_b v_b}{\dot{M}_a v_a},$$

where R_i is the distance between the WCR and star i (Usov 1992). The value of η is independent of orbit inclination.

From the relative positions of Aa, Ab, and the centroid of the radio emission in Fig. 7, we estimate $R_b/R_a \approx 0.7$. The stellar winds of the two stars are assumed to have reached their terminal velocities before colliding, considering the wide orbit, and we further assume that the terminal velocities of both components are similar (see the values quoted, for instance, in Table 1 of Muijres et al. 2012), then η reduces to a mass-loss rate ratio, leading to $\dot{M}_b \approx 0.5\dot{M}_a$.

In this work, we hesitate to use the shape of the WCR to estimate η. As Pittard & Dougherty (2006) (Sect. 4.3.3) show for WR 140, the emission in the WCR detected in VLBI is close to the stagnation point, and the opening angle has not reached the asymptotic value. They also noted the challenge of identifying the stagnation point relative to the stellar components due to opacity effects. In the best case, we can perhaps assume that the shape of the contact discontinuity (CD) between the two stellar winds (Canto et al. 1996) is represented by the radio emission.

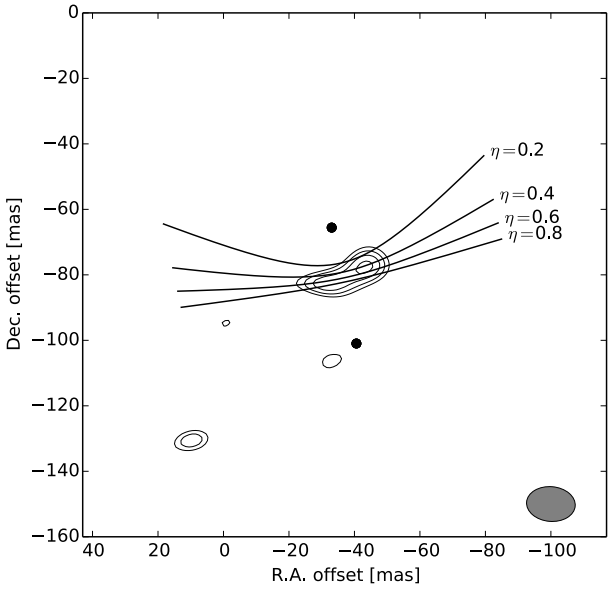

Fig. 8. HD 93129Aab system at 2.3 GHz, showing different η values. The black dots mark the position of the stars. The synthesized beam is shown in the bottom right corner.

In Fig. 8, the positions of the CD corresponding to different values of η are plotted relative to the emission detected in the LBA observation. The distance and angle between stars are known, so the only free parameters are the offsets with respect to the radio image and η. The η values that best match the radio source are between ∼0.4 and ∼0.6.

6.2. The binary nature of HD 93129A

Do HD 93129Aa and Ab form a gravitationally bound binary system? The system is being monitored in the OWN Survey project (Barbá et al. 2010). A radial velocity (RV) curve from preliminary data shows slight variations though no period has been determined yet. The putative low-amplitude RV variations may be due to a number of factors, including insufficient data over a potential orbital period, a very low-mass companion, or unfavorable orbital inclination (Barbá & Gamen, priv. comm.).

An argument in support of HD 93129Aab being a bound system is the small angular separation and the change in the rate at which the two stars are approaching one another. In the simplest scenario, if they are in the plane of the sky, with a separation of 26.5 mas (epoch 2013.09 from Sana et al. 2014) and at a distance of 2.5 kpc, they have a physical separation of only 66 AU, which implies a bound system for such massive stars. However, this strongly depends on the inclination being in the plane of the sky. More compelling is the increase in the rate at which the two stars are approaching one another. Based upon FGS and ACS data, between 1996 and 2009 the separation had been closing at approximately 2.4 mas yr^{-1}, but VLTI data shows this rate to have accelerated to 4.2 mas yr^{-1} between 2011.19 and 2013.09 (Sana et al. 2014), consistent with a binary system approaching periastron. The relative positions in Fig. 1 suggest either an orbital inclination close to 90 degrees or a nearly face-on orbit of high eccentricity. The results of the very preliminary orbit fits given in Sect. 3 favor the former hypothesis.

Table 4. Mass loss rates values derived for HD 93129A.

Reference	Method	Value $\times 10^5$ ($M_\odot$ yr^{-1})
Tar97	Hα profile	1.8
Tar97	Ultraviolet lines	2.08
Rep04	Hα profile	2.36
BK04	8.64 GHz continuum flux	$(f_T)^{3/4}$ 7.2†
This work	Separating T and NT fluxes	4.9††

Notes. $^{(\dagger)}$ (f_T) ϵ [0,1] ; $^{(\dagger\dagger)}$ see text.

References. Tar97: Taresch et al. (1997); Rep04: Repolust et al. (2004); BK04: Benaglia & Koribalski (2004).

6.3. The mass-loss rates of the HD 93129A system

HD 93129A has been the target of different studies aimed at deriving the mass-loss rate ($\dot{M}$)[6]. Assuming it was a single star, Taresch et al. (1997) estimated $\dot{M}$ of HD 93129A by fitting the Hα profile and also using a more complete spectral synthesis approach in the ultraviolet. These two approaches led to consistent values of 1.8×10^{-5} and 2.1×10^{-5} $M_\odot$ yr^{-1}, respectively. The authors considered that these values should be reduced by a factor $2^{3/4}$, a reduction of about 40%, if HD 93129A consisted of two very similar components. Using Hα line diagnostics exclusively, Repolust et al. (2004) derived a value of 2.4×10^{-5} $M_\odot$ yr^{-1} for the mass-loss rate, noting that the results could suffer from contamination by a companion star.

Benaglia & Koribalski (2004) present flux density measurements of the HD 93129A system from ATCA data at two frequencies, 4.8 and 8.64 GHz, and derived a spectral index $\alpha = -1.2 \pm 0.3$. Their interpretation was that both thermal and non-thermal emission were contributing to the radio emission. Wright & Barlow (1975) showed that the mass-loss rate of a star with a thermal wind can be expressed in terms of the radio flux density. If using the Wright & Barlow (1975) formulae and if f_T is the fraction of thermal emission at a given frequency, it is possible to express the mass-loss rate in terms of f_T as $\dot{M} = (f_T)^{3/4} \times 7.2 \times 10^{-5}$ $M_\odot$ yr^{-1} at $\nu = 8.64$ GHz for a stellar distance of 2.5 kpc. This leads to a mass-loss rate of $\approx 5 \times 10^{-5}$ $M_\odot$ yr^{-1} if $f_T = 0.5$.

At the epoch of the observations presented by Benaglia & Koribalski (2004), the stars Aa and Ab were ~50 mas apart in the plane of the sky (see Sect. 2). The angular resolution of the ATCA data at ~1 arcsec precludes separation of the contributions to the total flux of both stellar winds and a colliding-wind region. An estimate of the thermal emission from the two stellar winds can be obtained from the radio observations in Benaglia et al. (2006) from ATCA at 17.8 and 24.5 GHz. At these frequencies, non-thermal emission is negligible and can be disregarded to zeroth order. The total flux is then the sum of the thermal emission from the two stellar winds and is characterized by a spectral index of +0.6 (Wright & Barlow 1975). Consequently, the thermal contribution to the flux at lower frequencies can be derived by extrapolation and assuming no variations between 2003 (8.64 GHz data) and 2004 (17.8 GHz data). This leads to a thermal contribution at 8.64 GHz of 1.2 mJy, compared with a total flux of 2.00 ± 0.15 mJy (see Table 3), an $f_T \approx 0.6$, and $\dot{M} = 4.9 \times 10^{-5}$ $M_\odot$ yr^{-1}. Table 4 lists $\dot{M}$ values.

The main conclusion here is that mass-loss rate determinations are challenging when dealing with a binary system.

[6] For an overview of these mass-loss-rate determination techniques, including a comprehensive discussion of their advantages and limitations, we refer to the review by Puls et al. (2008).

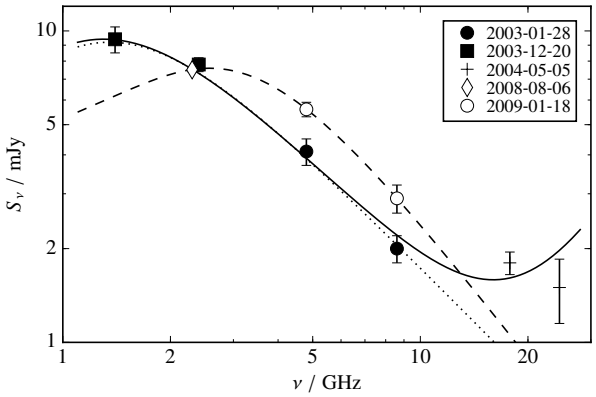

Fig. 9. Spectra of HD 93129A obtained from ATCA data at different epochs (see labels). The data from 2003 have been fitted with two different models: a free-free absorption (FFA, dotted line), and a FFA plus a thermal emission that also consider the 2004 data (solid line). The 2008–2009 data have been fitted with a FFA model (dashed line); see also Pittard & Dougherty (2006).

Considering the large number of binaries among O-type stars (see, e.g., Sana et al. 2014, and references therein), many observational determinations of $\dot{M}$ should certainly be viewed with caution, including those of HD 93129A.

6.4. Flux density variability of HD 93129A

The flux density measurements of HD 93129A derived from ATCA data (Table 3) cover frequencies from 1.4 to 24.5 GHz. Observations at 2.4, 4.8, and 8.6 GHz were obtained twice at different epochs. The two measurements at 2.4 GHz were observed in 2003 and 2008, and the fluxes agree within the uncertainties.

The fluxes at 4.8 GHz (from 2003 and 2009) differ by ~37%, increasing with time. Similarly, the 8.6 GHz fluxes at the same epochs differ by ~45%. In all the archival observations, relative errors are 10% or less. We checked for calibration errors in the individual datasets. For all of them, the flux calibrator was 1934-638, from which the flux scale of phase calibrators and source were bootstrapped.

The data indicate that the flux increased by a significant fraction compared to the uncertainties between 2003 and 2009. Such a trend is indeed anticipated if the system is approaching periastron passage (cf. WR 140, Dougherty et al. 2005). A synchrotron component that dominates the thermal emission from the stellar winds of the two stars can explain the measured flux densities. We modeled the data with a power-law spectrum with a low-frequency exponential cutof and computed two possible models. The first model fits the data from January 2003–December 2003, and the 2004 data at the higher frequencies (Fig. 9). It is assumed that the flux does not vary significantly within this range of time, given the separation of Aa to Ab in that period. These data are well-fit by a power law, with a turnover around 1.4 GHz. However, the data from 2008 and 2009 are modeled by a similar power-law spectrum but with a turnover at a slightly higher frequency. An additional thermal component is required to fit the data at 20 GHz. The spectral indices from the fits to the 2003-4 and 2008-9 data are, respectively, -1.03 ± 0.09 and -1.21 ± 0.03.

Up to now, the results from observations at high-energy spectral bands remain inconclusive in detecting emission from a WCR. In soft X-rays (below 10 keV), the work by Cohen et al. (2011) concluded that the X-ray spectrum is dominated by emission from the individual stellar winds in the system. On the other hand, Gagné et al. (2011) report a ratio between the X-ray and

bolometric luminosities (L_X/L_{bol}) of 1.3×10^{-7}. This value suggests that only a small contribution of the X-rays come from the colliding-wind region. We expect to see colliding-wind binaries made of very early-type stars with no bright X-ray emission in excess of the canonical L_X/L_{bol} value of $\sim 10^{-7}$. For very early-type stars with strong and dense winds like the members of HD 93129A, the individual X-ray emission should be somewhat fainter than suggested by the canonical ratio (De Becker 2013; Owocki et al. 2013). A low emission measure of a WCR due to a large stellar separation on top of such an underluminous wind emission leads therefore to a not very high overall L_X/L_{bol} ratio.

HD 93129A is fairly close to the Fermi source 1FGL J1045.2−5942 (in the 0.1–100 GeV energy range). This source is associated with η Car, the only PACWB identified on the basis of γ-ray emission. It seems very unlikely that HD 93129A contributes to the emission detected by Fermi, as clarified by Abdo et al. (2010). At even higher energies, no TeV source has been found at the position of HD 93129A in the TevCat catalog[7], even when considering newly announced sources and source candidates. We conclude that there is no known γ-ray source associated with HD 93129A. Observations with the forthcoming Cherenkov Telescope Array, with unprecedented sensitivity and source location techniques, will surely provide useful constraints to help understand the high energy phenomena in these objects better.

7. Summary and conclusions

An LBA observation of the massive binary HD 93129A detected an extended and arguably curved radio emission component with a flux density of 2.9 mJy at 2.3 GHz between the two components Aa and Ab. Following a detailed analysis of recent high angular resolution astrometry of the system, we provide compelling evidence that the radio emission component is coincident with the expected position of a wind interaction region between components Aa and Ab and suggest a wind-momentum ratio of ∼0.5.

Historic ATCA observations of the HD 93129A system from 1 to 25 GHz, reduced again in a uniform way, show that the flux increased between 2003-4 and 2008-9, both epochs being well fit by a power-law spectrum with a steep spectral index. Similar increases in flux have been seen in other systems as they approach periastron. Thus, the results presented in this paper lend significant additional support to the idea that wind-collision regions are the sites where relativistic particles are accelerated in particle-accelerating colliding-wind binaries.

Very Long Baseline Interferometer (VLBI) observations of particle-accelerating colliding-wind binaries specifically help to quantify the properties of the non-thermal radio emission. Such measurements are crucial for models aimed at reproducing the particle acceleration and non-thermal physics at work in these objects. VLBI observations of the HD 93129A system across a wide frequency range will allow more accurate properties of the spectrum to be derived, hence the properties of the relativistic electron populations involved in the synchrotron emission process, and potentially reveal associations between flux variations and changes in the properties of the wind-collision region.

In parallel, new ATCA observations, preferably simultaneous across all the observing frequencies are necessary to obtain accurate total fluxes. Repeated observations during the approach to the putative periastron passage will reveal whether the flux increases as observed in other PACWB systems at this phase of the orbit.

Acknowledgements. The authors thank an anonymous referee for detailed comments, C. Phillips and A. Tzioumis for their work in a preliminary stage of the study, A. López-Sánchez for providing some of the ATCA observations, Rodolfo Barbá, Roberto Gamen, Ed Fomalont, Jamie Stevens, and very especially G. Vila and N. Casco for help with the orbits. P.B. is supported by the ANPCyT PICT- 2012/00878 and UNLP G11/115 project. B.M. acknowledges support by the Spanish Ministerio de Economía y Competitividad (MINECO) under grants AYA2013-47447-C3-1-P and BES-2011-049886. This study was partially supported by NASA through grant GO-10898 from the Space Telescope Science Institute, which is operated by AURA, Inc., under NASA contract NAS 5-26555. The research has made use of the Washington Double Star Catalog maintained at the US Naval Observatory.

References

Abdo, A. A., Ackermann, M., Ajello, M., et al. 2010, ApJ, 723, 649
Barbá, R. H., Gamen, R., Arias, J. I., et al. 2010, in Rev. Mex. Astron. Astrofis. Conf. Ser., 38, 30
Benaglia, P., & Koribalski, B. 2004, A&A, 416, 171
Benaglia, P., & Romero, G. E. 2003, A&A, 399, 1121
Benaglia, P., Koribalski, B., & Albacete Colombo, J. F. 2006, PASA, 23, 50
Benaglia, P., Dougherty, S. M., Phillips, C., Koribalski, B., & Tzioumis, T. 2010, in Rev. Mex. Astron. Astrofis. Conf. Ser., 38, 41
Benedict, G. F., McArthur, B. E., Feast, M. W., et al. 2007, AJ, 133, 1810
Canto, J., Raga, A. C., & Wilkin, F. P. 1996, ApJ, 469, 729
Cohen, D. H., Gagné, M., Leutenegger, M. A., et al. 2011, MNRAS, 415, 3354
Contreras, M. E., Rodríguez, L. F., Tapia, M., et al. 1997, ApJ, 488, L153
De Becker, M. 2007, A&ARv 14, 171
De Becker, M. 2013, New Astron., 25, 7
De Becker, M., & Raucq, F. 2013, A&A, 558, A28
Dougherty, S. M., & Pittard, J. M. 2006, in Proc. of the 8th European VLBI Network Symp., 49
Dougherty, S. M., Beasley, A. J., Claussen, M. J., Zauderer, B. A., & Bolingbroke, N. J. 2005, ApJ, 623, 447
Eichler, D., & Usov, V. 1993, ApJ, 402, 271
Gagné, M., Fehon, G., Savoy, M. R., et al. 2011, ApJS, 194, 5
Høg, E., Fabricius, C., Makarov, V. V., et al. 2000, A&A, 355, L27
Jefferys, W. H., Fitzpatrick, M. J., & McArthur, B. E. 1987, Celest. Mech., 41, 39
Maíz Apellániz, J., Walborn, N. R., Morrell, N. I., et al. 2008, in Rev. Mex. Astron. Astrofis. Conf. Ser., 33, 55
Mason, B. D., Gies, D. R., Hartkopf, W. I., et al. 1998, AJ, 115, 821
Muijres, L. E., Vink, J. S., de Koter, A., Müller, P. E., & Langer, N. 2012, A&A, 537, A37
Nelan, E. P. 2014, Fine Guidance Sensor Instrument Handbook, Version 22.0 (Baltimore, MD: STScI)
Nelan, E. P., & Bond, H. E. 2013, ApJ, 773, L26
Nelan, E. P., Walborn, N. R., Wallace, D. J., et al. 2004, AJ, 128, 323
Nelan, E. P., Walborn, N. R., Wallace, D. J., et al. 2010, AJ, 139, 2714
O'Connor, E. P., Dougherty, S. M., Pittard, J. M., & Williams, P. M. 2005, in Massive Stars and High-Energy Emission in OB Associations, eds. G. Rauw, Y. Nazé, R. Blomme, & E. Gosset, 81
Ortiz-León, G. N., Loinard, L., Rodríguez, L. F., Mioduszewski, A. J., & Dzib, S. A. 2011, ApJ, 737, 30
Owocki, S. P., Sundqvist, J. O., Cohen, D. H., & Gayley, K. G. 2013, MNRAS, 429, 3379
Payne, C. H. 1927, Harvard College Observatory Bulletin, 846, 10
Pittard, J. M., & Dougherty, S. M. 2006, MNRAS, 372, 801
Puls, J., Vink, J. S., & Najarro, F. 2008, A&ARv, 16, 209
Repolust, T., Puls, J., & Herrero, A. 2004, A&A, 415, 349
Roeser, S., Demleitner, M., & Schilbach, E. 2010, AJ, 139, 2440
Sana, H., Le Bouquin, J.-B., Lacour, S., et al. 2014, ApJS, 215, 15
Smart, W. M. 1960, Text-book on spherical astronomy (CUP)
Sota, A., Maíz Apellániz, J., Morrell, N. I., et al. 2014, ApJS, 211, 10
Taresch, G., Kudritzki, R. P., Hurwitz, M., et al. 1997, A&A, 321, 531
Usov, V. V. 1992, ApJ, 389, 635
Walborn, N. R. 1982, AJ, 87, 1300
Walborn, N. R. 1995, Rev. Mex. Astron. Astrofis. Conf. Ser., 2, 51
Walborn, N. R., Howarth, I. D., Lennon, D. J., et al. 2002, AJ, 123, 2754
Williams, P. M., Dougherty, S. M., Davis, R. J., et al. 1997, MNRAS, 289, 10
Wright, A. E., & Barlow, M. J. 1975, MNRAS, 170, 41

[7] http://tevcat.uchicago.edu/